

# We are IntechOpen, the world's leading publisher of Open Access books Built by scientists, for scientists

6,900

Open access books available

186,000

International authors and editors

200M

Downloads

Our authors are among the

154

Countries delivered to

TOP 1%

most cited scientists

12.2%

Contributors from top 500 universities



WEB OF SCIENCE™

Selection of our books indexed in the Book Citation Index  
in Web of Science™ Core Collection (BKCI)

Interested in publishing with us?  
Contact [book.department@intechopen.com](mailto:book.department@intechopen.com)

Numbers displayed above are based on latest data collected.  
For more information visit [www.intechopen.com](http://www.intechopen.com)



# Toward On-Demand Generation of Entangled Photon Pairs with a Quantum Dot

*Arash Ahmadi, Andreas Fognini and Michael E. Reimer*

## Abstract

The generation of on-demand, optimally entangled photon pairs remains one of the most formidable challenges in the quantum optics and quantum information community. Despite the fact that recent developments in this area have opened new doors leading toward the realization of sources exhibiting either high brightness or near-unity entanglement fidelity, the challenges to achieve both together persist. Here, we will provide a historical review on the development of quantum dots (QDs) for entangled photon generation, with a focus on nanowire QDs, and address the latest research performed on nanowire QDs, including measuring entanglement fidelity, light-extraction efficiency, dephasing mechanisms, and the detrimental effects of detection systems on the measured values of entanglement fidelity. Additionally, we will discuss results recently observed pertaining to resonant excitation of a nanowire QD, revealing the potential of such sources to outperform spontaneous parametric down-conversion (SPDC) sources, providing a viable solution to the current challenges in quantum optics and quantum information.

**Keywords:** nanowire quantum dot, entanglement, dephasing, resonant two-photon excitation, fine-structure splitting

## 1. Introduction

Entangled photon pairs are one of the key elements for research and in emerging quantum applications with successful results in quantum foundations [1, 2], quantum communication [3–5], and quantum information [6–8]. Thus far, nonlinear crystals exhibiting spontaneous parametric down-conversion (SPDC) [9–11] have been the main source of generating entangled photon pairs for use in these areas. This type of source results in photon pairs that exhibit near-unity entanglement fidelity, high degrees of single-photon purity and indistinguishability in each emission mode, and high temporal correlation. Moreover, these sources perform at or near room temperature. However, there are fundamental limitations to such sources, which limit their performance and scalability for use in quantum photonics; an ideal source is imperative for optimal performance. One key feature of an ideal source of entangled photons is the ability to perform on-demand, i.e., source triggering and extraction of light must be possible with near-unity efficiency. SPDC sources follow a stochastic process and therefore generate entangled photon pairs at random. Moreover, the probability of multiphoton generation follows a Poisson distribution, and thus entanglement

fidelity, single-photon purity, and photon indistinguishability [12] degrade when the pump power is increased [13]. As a result, these sources only operate at extremely low pair-production efficiencies,  $\epsilon_p < 1\%$ , per excitation pulse [14]. Hence, engineering and realizing an ideal source of entangled photons is necessary for the successful future of entangled photon pairs for use in quantum photonics, a future made brighter by semiconductor quantum dots (QDs).

Semiconductor quantum dots [15] are capable of generating pairs of entangled photons based on a process called the biexciton ( $XX$ )-exciton ( $X$ ) cascade [16]; this cascade process is shown in **Figure 1**. The  $|XX\rangle$  state is composed of two electron-hole ( $e-h$ ) pairs in the QD's lowest energy level, i.e.,  $s$ -shell. Each of these pairs possesses an angular momentum  $j_z$  with the superposition of  $j_z = \pm 1$ . From the  $|XX\rangle$  state, there are two recombination pathways through the intermediate  $|X\rangle$  state. Upon recombination, the  $e-h$  pair will emit either a left,  $|L\rangle$ , or right,  $|R\rangle$ , circularly polarized photon corresponding to  $j_z = +1$  or  $j_z = -1$ , respectively, and the QD final state at this step will be in the  $|X\rangle$  state. This transition,  $|XX\rangle \rightarrow |X\rangle$ , is referred to as the neutral biexciton,  $XX$ , transition. Relaxation to the ground state occurs by the recombination of the remaining  $e-h$  pair in the  $|X\rangle$  state. The latter transition, i.e.,  $|X\rangle \rightarrow |G\rangle$ , is referred to as the neutral exciton,  $X$ , transition. This recombination will emit a photon with a polarization perpendicular to that of the first photon ( $XX$ ), i.e.,  $|L\rangle_{XX} \rightarrow |R\rangle_X$  and  $|R\rangle_{XX} \rightarrow |L\rangle_X$ . At the end of the process, the two emitted photons will be in the polarization entangled state [16]:

$$|\Psi\rangle = \frac{1}{\sqrt{2}}(|RL\rangle + |LR\rangle). \quad (1)$$

Over the past three decades, QDs have been extensively studied with recent advancements, as compared to other solid state quantum emitters [18–21], and have produced sources which exhibit features closest to an ideal photon source [22]. The first generation of QDs was self-assembled [23–25], which resulted in QDs with various sizes and imperfect symmetry due to the random nature of the formation process [13]. Moreover, since the bulk semiconductor material possessed a high

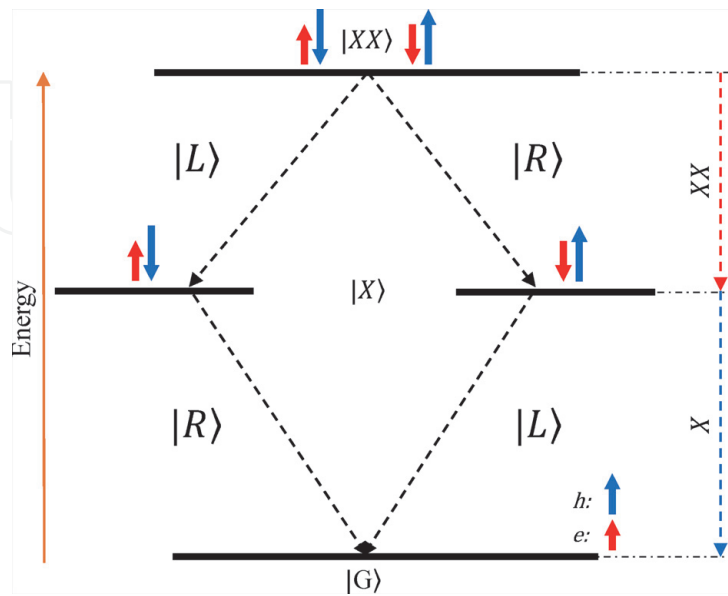


**Figure 1.**

The  $XX$ - $X$  cascade. In the  $|XX\rangle$  state, holes with  $j_z = \pm \frac{3}{2}$  and electrons with  $j_z = \pm \frac{1}{2}$  are paired, resulting in exciton states with  $j_z = \pm 1$ . The two  $e-h$  pairs will then lead to two different recombination pathways, with the final state being a superposition of these two paths, i.e.,  $|\Psi\rangle = \frac{1}{\sqrt{2}}(|RL\rangle + |LR\rangle)$ . For a more detailed description of the QDs' electronic structure, please refer to ref. [17].

refractive index, these self-assembled QDs typically suffered from isotropic emission and total internal reflection at the semiconductor-air interface and thus exhibited a low light-extraction efficiency of  $\sim 1\%$  [26].

Recent developments in micro- and nanoscale crystal growth and fabrication have resulted in structures which have improved the performance of QDs considerably. Enhancement of the spontaneous emission of QDs was first achieved by coupling an ensemble of QDs [27], and later a single QD, to a micro-cavity [28]. More recently, the coupling of QDs to micro-pillar cavities has achieved light-extraction efficiencies as high as 80% [29]. Also, such structures allow for proper control of the charge noise around the QD and thus the suppression of detrimental dephasing processes from the moving charge carriers. Excitingly, as a result, photons with  $> 99\%$  indistinguishability and single-photon purity have been reported [30].

However, such performance comes at a price. Due to Coulomb interactions [17],  $XX$  and  $X$  emission lines are separated in energy by an amount referred to as the  $XX$  binding energy,  $\Delta_{XX-X}$ . Within a typically used cavity with a quality factor of  $Q \sim 10,000$ , which is tuned to photons with the wavelength  $\lambda \sim 1\mu\text{m}$ , the cavity has a bandwidth of  $\sim 10\mu\text{eV}$ . This small bandwidth is far less than a typical  $XX$  binding energy of  $\Delta_{XX-X} \sim 1\text{meV}$  [31]. Therefore, either the  $X$  or the  $XX$  transition lines can be coupled to the fundamental mode of the cavity, but not both as needed for a high-efficiency entangled photon source. Furthermore, to avoid suboptimal entanglement, coupling to the fundamental mode of the cavity should be polarization-independent. Otherwise, one decay path in the cascade process would gain a stronger weight [32]. In an attempt to overcome these challenges, three studies have made considerable gains. Dousse et al. [32] fabricated a micropillar cavity molecule and successfully tuned both  $XX$  and  $X$  transitions to separate cavity modes in the molecule. Impressively, the fabricated device was shown to improve the pair-extraction efficiency ( $\epsilon_e$ ) by three orders of magnitude,  $\epsilon_e = 12\%$ , as compared to a bare self-assembled QD; yet despite this, the source still generates poorly entangled photon pairs with a measured fidelity of  $\mathcal{F} = 67\%$ . Other research by Chen et al. [26] showed the successful fabrication of a broadband dielectric antenna, which enables a pair-extraction efficiency of 37.2%, low multiphoton emission  $g^{(2)}(0) \approx 0.002$ , and entanglement fidelity,  $\mathcal{F} = 90\%$ ; however, the emission profile deviates from a Gaussian, and photon indistinguishability of such sources is yet to be measured. Additionally, Wang et al. [33] have engineered a circular Bragg grating bull's-eye cavity around a single QD showing a pair-extraction efficiency,  $\epsilon_e = 36.6\%$ , and an entanglement fidelity,  $\mathcal{F} = 90\%$ . Despite these impressive gains, still none exhibit the promise of quantum dots in realizing an ideal entangled photon source, showing near-unity entanglement fidelity and pair-extraction efficiency.

Another important feature of QDs affecting the measured entanglement is the fine-structure splitting (FSS) of the  $|X\rangle$  state, which is caused by the exchange interaction of the electron and hole in the  $e-h$  pair, together with geometrical asymmetries of the QD [34, 35]. As a result, in the  $XX-X$  cascade, there is a precession between the two recombination pathways in the  $|R\rangle/|L\rangle$  basis (**Figure 2(a)**), and a non-degeneracy in energy of the two pathways in the  $|H\rangle/|V\rangle$  basis will appear (**Figure 2(b)**). Therefore, the two-photon quantum state described by Eq. (1) will change into:

$$\begin{aligned} |\tilde{\Psi}\rangle &= \frac{1}{\sqrt{2}} \left( |HH\rangle + e^{i\frac{\delta}{2\hbar}t} |VV\rangle \right) \\ &= \cos\left(\frac{\delta}{2\hbar}t\right) |\Psi\rangle + i \sin\left(\frac{\delta}{2\hbar}t\right) |\Phi\rangle, \end{aligned} \quad (2)$$

where  $|\Psi\rangle$  is the state described by Eq. (1),  $|\Phi\rangle = \frac{1}{\sqrt{2}}(|RR\rangle + |LL\rangle)$ , and  $\delta = \text{FSS}$ .

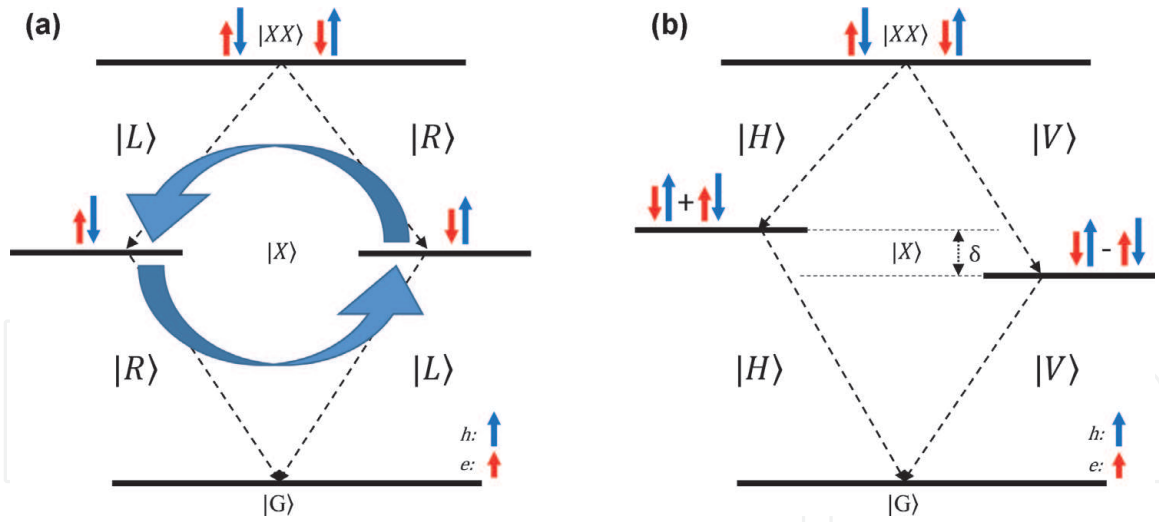


**Figure 2.**

*XX-X cascade in the presence of FSS. (a)  $|R\rangle$  and  $|L\rangle$  basis will be mixed and a precession between the two pathways will be observed. (b) In the  $|H\rangle/|V\rangle$  basis, the transition energies will be split by  $FSS = \delta$ .*

Due to the random nature of the growth process, self-assembled QDs have long suffered from large base asymmetries, which resulted in FSS values larger than the X emission linewidth. This feature will lead to the introduction of a which-path information in the  $XX - X$  cascade that will degrade the entanglement between the two emitted photons. For this reason, the early measurements on entanglement in QDs [36, 37] only led to detection of classical correlations; nonclassical correlations were only observed by improving the growth techniques and choosing QDs with  $FSS \approx 0$  [38, 39]. In the recent past, several techniques have been proposed and demonstrated in order to erase the FSS of QDs using electric fields [40–42], strain [43], and an optical approach not requiring nanofabrication [44]. However, as we show further along in the chapter, in order to reveal the effect of FSS on entanglement fidelity of the emitted photon pair, a delicate understanding of the detection system is also required. A recent study by Fognini et al. [45] shows that it is possible to measure near-unity entanglement fidelity even in the presence of finite FSS.

To reveal the true potential of QDs, proper excitation schemes are needed in addition to engineering sophisticated photonic structures. Until recently, off-resonant excitation had been widely used to generate entangled and single photons from QDs in photonic structures. This scheme excites charge carriers to energy levels above the bandgap of the host semiconductor, and relaxation of the resulted  $e - h$  pairs to the QD's  $s$ -shell, mediated by interactions with phonons, leads to the emission of entangled photons. Admittedly, implementing this scheme is relatively straightforward, as the large difference in the frequencies of the excitation laser and the emitted photons allow for simple filtration of the reflected laser light. The excess of charge carriers and their interaction with phonons will lead to detrimental effects such as inhomogeneous broadening of emission lines [46], multiphoton emission caused by re-excitation processes [47], increased jitter in emission time [48], and dephasing [45].

Direct population of  $|XX\rangle$  is forbidden due to optical selection rules. However, observation of resonant two-photon absorption in photoluminescence excitation spectroscopy of QDs [49] has recently led to development of a resonant two-photon excitation (TPE) scheme [50–52], which allows for coherent population of the  $|XX\rangle$  state. In order to perform this scheme (**Figure 3**), a linearly polarized excitation pulse is tuned to a virtual state with an energy halfway between that of the ground state,  $E_{|G\rangle}$ , and biexciton state,  $E_{|XX\rangle}$ . This virtual state can also be thought of as a transition level between that of the neutral exciton and that of the neutral biexciton transitions. In other words,  $|XX\rangle$  is coherently populated by a laser pulse, which is

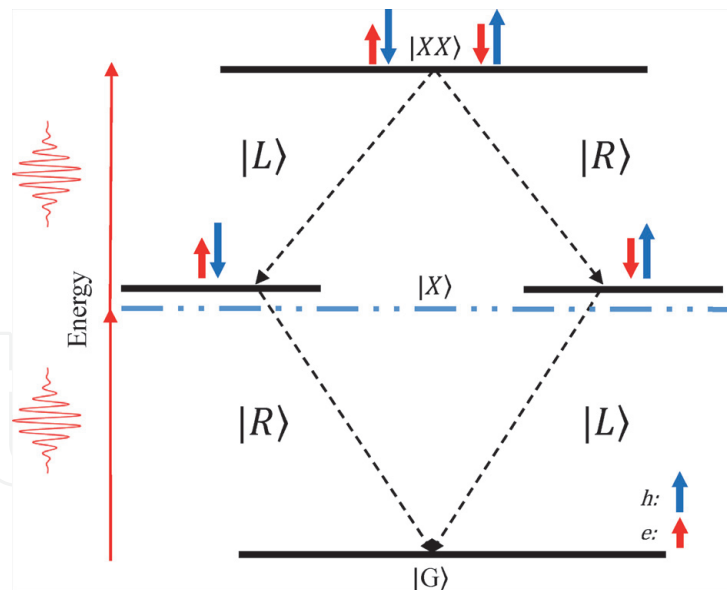


**Figure 3.** Schematics of resonant TPE. A linearly polarized pulse is tuned to a virtual state halfway between  $X$  and  $XX$  transitions (the dashed blue line); and the  $|XX\rangle$  is coherently populated via a two-photon absorption process.

resonant to neither  $X$  nor  $XX$  transitions. This method can lead to near-unity population of the  $|XX\rangle$  state [53] and an extreme suppression of multiphoton emission of  $X$  and  $XX$  transitions [54].

In this review, we focus on attempts to improve the performance of entangled photon generation in by embedding them in photonic nanowires, as well as the effects of different excitation schemes in the performance of such sources. Additionally, we will also cover the improvements achieved in photon extraction efficiency, reduction of the dephasing processes, suppression of multiphoton emission, and enhancing entanglement fidelity of nanowire QD based entangled photon sources.

## 2. Nanowire QDs

Embedding QDs in tapered nanowires was initially developed by using top-down approaches via reactive-ion etching [55, 56]. Such photonic structures allow for coupling of the QD emission to the waveguide's fundamental mode in a broad range of wavelengths,  $\Delta\lambda \approx 70\text{nm}$ . Claudon et al. [55] managed to achieve a light-extraction efficiency of  $\epsilon \approx 72\%$ ; however, top-down approaches are not flawless. Defects are left at the surface of the nanowire due to etching of the substrate using reactive ions, and additionally there is limited control in the positioning of the QDs at the symmetry axis of the nanowire. It is important to note that these flaws lead to suboptimal quality in the ultimate brightness of the source. As an alternative growth approach in attempt to overcome these issues, pure wurtzite InP nanowires were grown with a bottom-up growth approach and the quantum dot was placed on the nanowire axis to ensure good ( $\sim 95\%$ ) coupling between the quantum dot and fundamental mode of the nanowire waveguide.

### 2.1 Bottom-up grown tapered wurtzite nanowire QDs

A novel bottom-up approach to growing tapered nanowires was used in the work by Reimer et al. [57]. This innovative approach allowed, for the first time, the positioning of a QD on the symmetry axis of the nanowire and at a desired height with a precision of  $\sim 100\text{ nm}$  (Figure 4). In this method, the growth of the

nanowire core, InP, is initiated by a gold particle which defines the core of the nanowire and ultimately the size of the QD,  $D \approx 20 - 30\text{nm}$ . After reaching the desired height, arsine is introduced to the growth chamber, and the QD, InAsP, is grown. Then, by changing the growth conditions, the nanowire is grown radially in order to create a shell  $D \approx 220\text{nm}$ , which facilitates the waveguide effect. In the last phase of growth, the conditions are changed once again to achieve an ideal tapering at the nanowire tip with an angle of  $\theta < 2^\circ$ , which results in minimal internal reflection for the emitted photons leaving the nanowire.

## 2.2 Optical properties

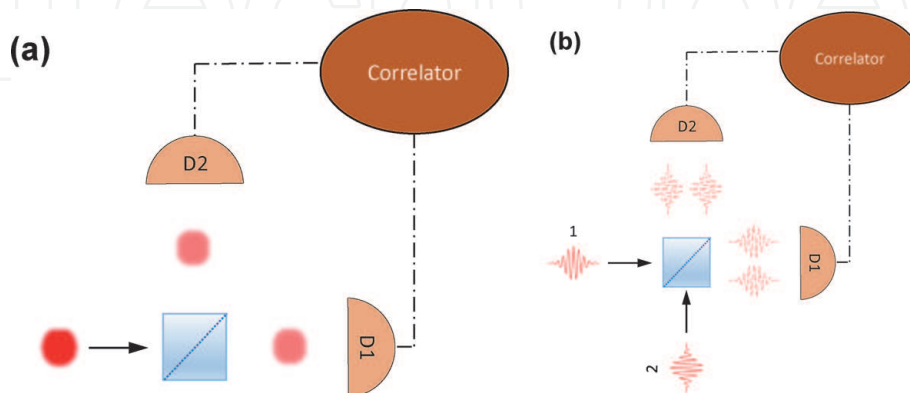
In terms of brightness, a value of  $\epsilon = 43(4)\%$  for success probability of single-photon extraction at the first lens has been reported [46]. However, theoretically these sources allow for single-photon extraction efficiencies up to  $\epsilon = 97\%$ , which can be achieved by perfect tapering of the nanowire,  $\theta = 1^\circ$ , placing the nanowires on top of a flawless mirror and placing the QD at the correct height in order to create perfect constructive interference [57]. In terms of multiphoton emission (**Box 1**), second-order correlation,  $g^{(2)}(0)$ , measurements yield values  $< 1\%$  [45, 46], showing a true single-photon emitter. The emitted photons exhibit extremely narrow linewidths,  $\delta\omega < 1\text{GHz}$ , with coherence lengths exceeding 1ns. Furthermore, a high level of visibility in a Hong-Ou-Mandel (HOM) measurement,  $V = 85\%$ , has been observed, indicating highly indistinguishable photons [46]. Moreover, there is a close to perfect overlap,  $98.8\% \pm 0.1\%$ , between the far-field emission profile of these nanowires QDs and a Gaussian emission profile of a

### 1. Hanbury Brown and Twiss (HBT) setup

In order to quantify the multiphoton emission of a source, the second-order correlation function is measured based on a setup first introduced by Hanbury Brown and Twiss [59] (**Figure a**). In this method, the light emitted from the source is sent to a beam splitter and then detected by two single-photon detectors D1 and D2. By correlating the intensities recorded by the two detectors in different time bins, one can gain information about the emission pattern of the source. Considering the particle nature of photons, if the source emits one and only one photon in each emission mode upon excitation, there will be no simultaneous detection on the two detectors; in other words, there will not be any correlation at zero time delay:

$$g^{(2)}(0) = \frac{\langle n_1(t)n_2(t) \rangle}{\langle n_1(t) \rangle \langle n_2(t) \rangle} = 0, \quad (3)$$

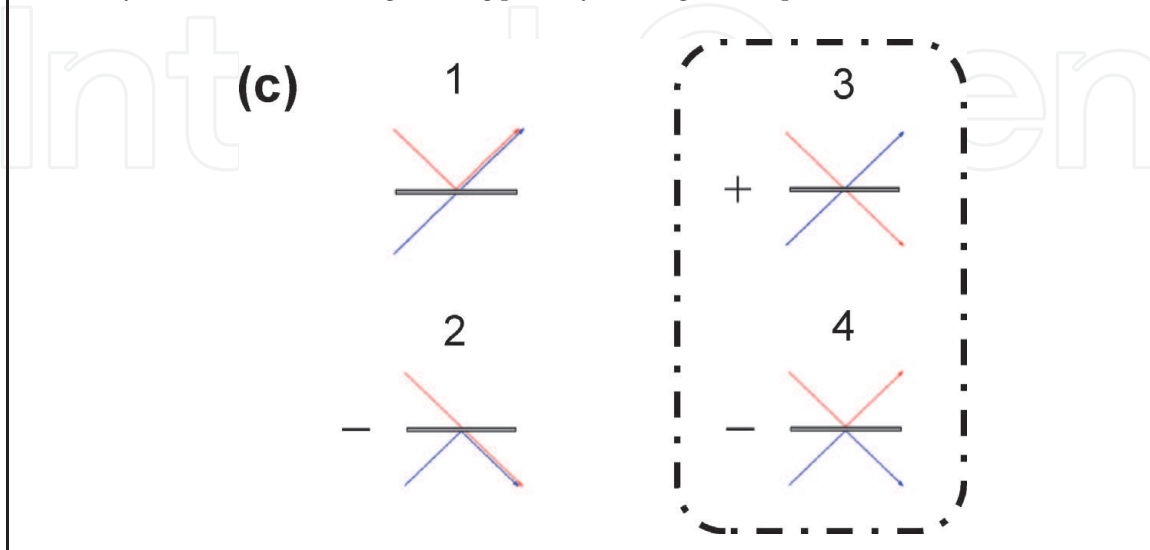
with  $n_i(t)$  being the number of photons detected by detector  $i$  ( $i = 1, 2$ ) at time  $t$ .



### 2. Hong-Ou-Mandel setup

In addition to single-photon emission, for an ideal entangled photon source, the emitted photons in each mode should exhibit perfect indistinguishability. For measuring this feature, the Hong-Ou-Mandel setup is used. Using a setup similar to that the HBT (**Figure b**) and considering the wave nature of the photons, a HOM measurement enables one to test the degree of indistinguishability of the successive

photons. In this scenario, two successive photons are brought together at the beam splitter for interference. Now, at the beam splitter, four different possibilities exist (**Figure c**); photon 1 may be reflected and photon 2 transmitted (case 1), photon 1 may transmit and photon 2 be reflected (case 2), both may transmit (case 3), and, lastly, both may be reflected (case 4). With reflection from the two sides of the beam splitter differing in a  $\pi$  phase shift, the third and the fourth cases are physically identical except for a general phase. Therefore, in the interference of the two photons, these two cases will cancel out, leaving only the options with the two photons going to either D1 or D2. Building a histogram out of the correlations of the two detectors, similar to the second-order correlation measurement, exhibits zero coincidence counts at zero time delay for the case of a source generating perfectly indistinguishable photons in each mode.



**Box 1.**

*Measuring multiphoton emission and photon indistinguishability of entangled photon sources.*

single-mode fiber; in practice, these sources have resulted in a coupling efficiency over 93% into a single-mode fiber [58]. Impressively, this feature then allows for possibilities in long-distance fiber-based quantum communication with high efficiency through low-loss communication channels.

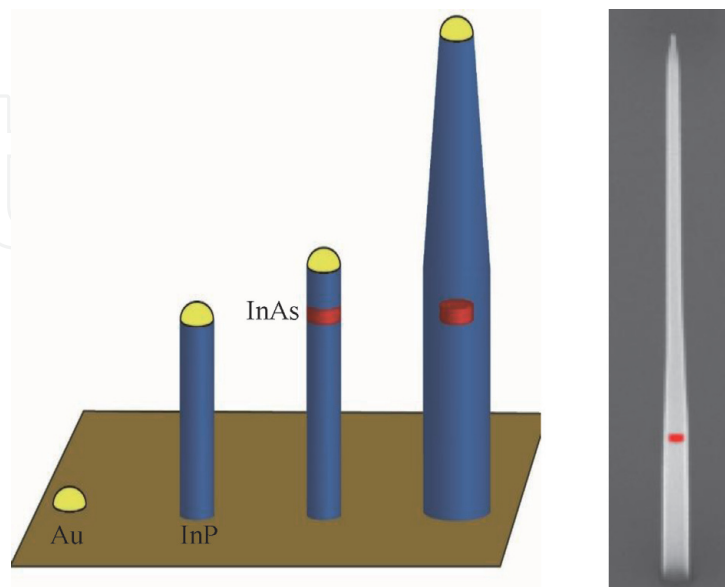


**Figure 4.**

*Schematic of the bottom-up nanowire growth process and SEM image of a tapered nanowire (right). The growth process is initiated by a gold particle, which defines the dimensions of the QD. After the quantum dot is grown the waveguide shell and the tapered tip are fabricated around the QD by controlling the growth parameters. This growth process ensures that the QD is placed on-axis of the tapered nanowire waveguide for efficient light extraction.*

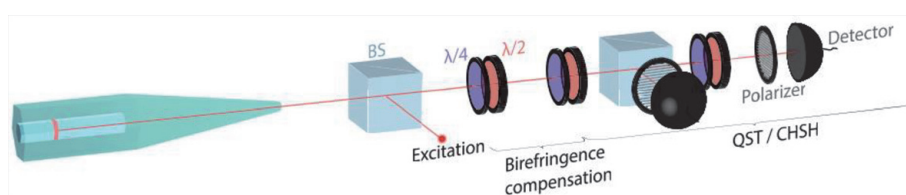
## 2.3 Entanglement measurements

Following the method introduced by James et al. [60], the first results in measuring the degree of entanglement in bottom-up grown nanowire QDs were reported in 2014 by Versteegh et al. [61]. In this work, using an above-bandgap excitation scheme, the fidelity of the emitted  $XX - X$  pairs to a maximally entangled state was found to be  $F = 0.859 (\pm 0.006)$ , with a concurrence equal to  $C = 0.80 (\pm 0.02)$ , under strong post-selection conditions. The fidelity is reduced to  $0.765 \pm 0.002$  with inclusion of 100% of the emitted photons. By changing the excitation conditions to excite the QD at the wurtzite InP nanowire bandgap, Jöns et al. [62] enhanced the fidelity of the same source as used by Versteegh et al. [61] to  $F = 0.817 \pm 0.002$  by including all of the collected photon pairs. This strong degree of entanglement allowed Jöns et al. [62] to perform a Bell type inequality violation test, specifically the Clauser-Horne-Shimony-Holt (CHSH) measurement [63]. The CHSH measurement yielded a violation of Bell's inequality by 25 standard deviations, clearly showing the promising features of bottom-up nanowire QDs for secure quantum communication purposes. The experimental setup can be seen in **Figure 5**. Initially, a pair of  $\lambda/2$  and  $\lambda/4$  waveplates corrects for the birefringence observed in the nanowire, causing the entangled state to rotate to an elliptical state instead of the expected  $|\Psi\rangle = \frac{1}{\sqrt{2}}(|HH\rangle + |VV\rangle)$  [61]. The stream of emitted photons are separated by a 50/50 beam splitter and sent to two separate detectors tuned to the specific wavelengths of the  $X$  and  $XX$ . In order not to be affected by the phase introduced when photons hit the reflecting surface of the beam splitter, the  $\lambda/2$  and  $\lambda/4$  waveplates used for projection measurements are aligned along the transmission path [62].

It is important to note that neither of the above-mentioned works addresses the ultimate entanglement fidelity achievable for nanowire QDs. In addition to the projection measurements, a more in-depth analysis is needed in order to reveal the underlying physical mechanisms such as dephasing due to nuclear spins and charge carriers through spin-flip processes. Moreover, the effect of  $FSS$  on the measured value of entanglement fidelity deserves more care, since, even though lifting of the degeneracy between the two decay paths in the  $XX - X$  cascade can be interpreted as an introduction of a which-path information, the effect is purely unitary, and the precession shall not destroy the entanglement alone. Here, the detection apparatus will play a major role regarding the effect of  $FSS$  on the entanglement fidelity.

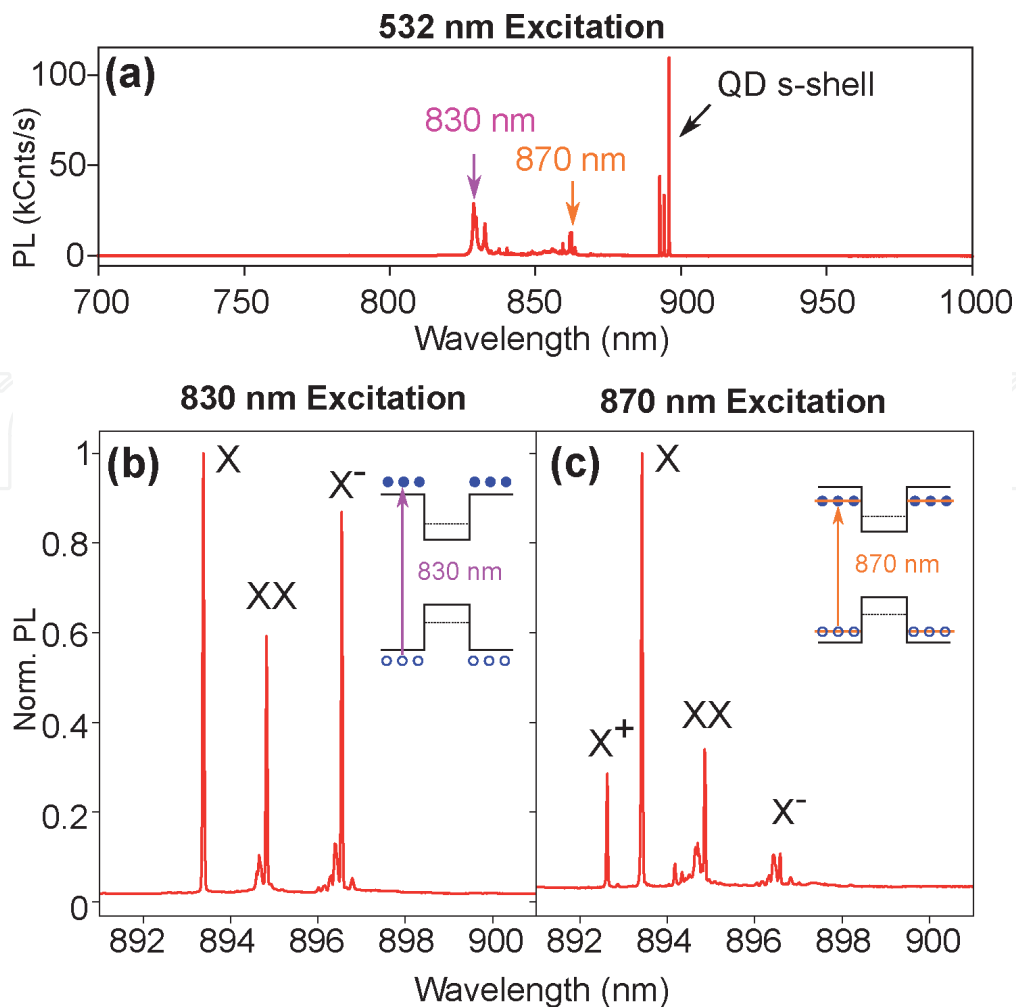
### 2.3.1 Dephasing-free entanglement in nanowire QDs

In an attempt to shed light on these finer aspects of generation of entangled photons in nanowire QDs, Fognini et al. [45] studied an InAsP QD embedded in an InP photonic nanowire, revealing the effects of dephasing,  $FSS$ , and imperfections of the detection system on the values achieved for entanglement fidelity.



**Figure 5.**

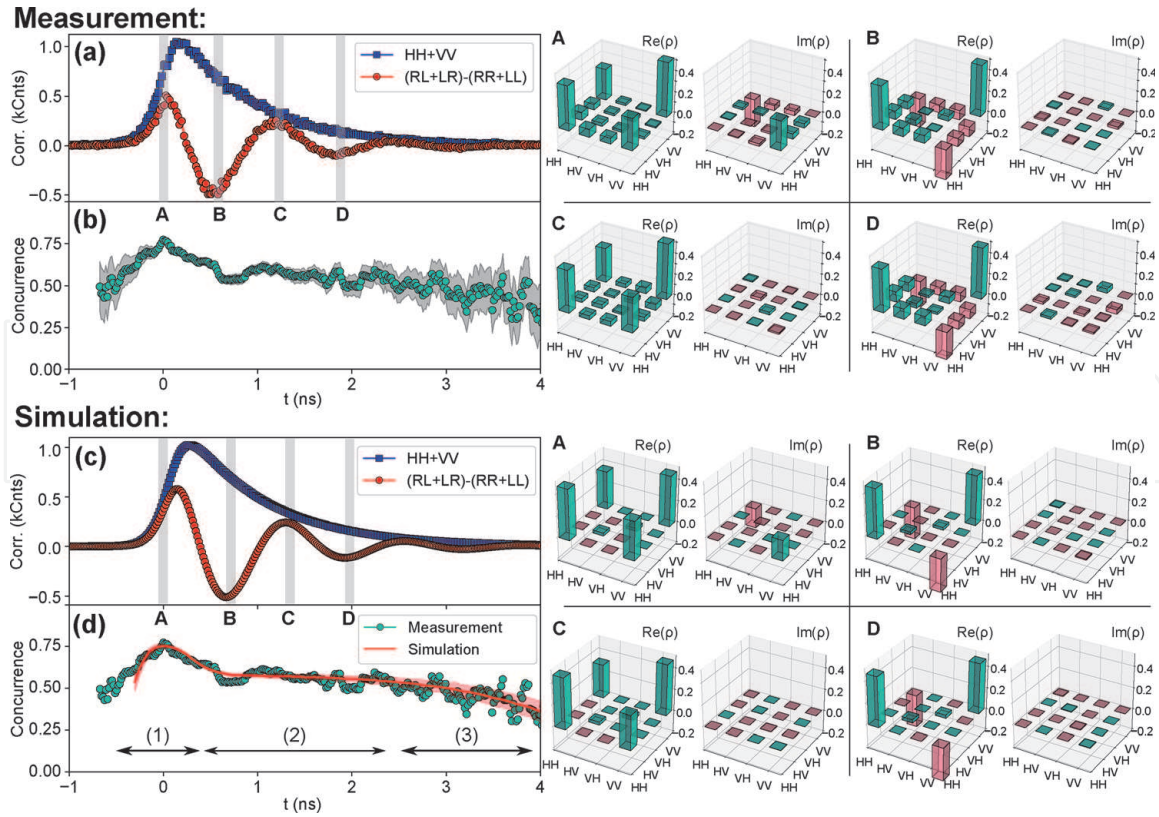
*Two-photon quantum state tomography setup. The setup consists of two pairs of  $\lambda/4$ - $\lambda/2$  wave plate sets, which combined with a pair of polarizers perform the projection measurements. A combination of  $\lambda/2$  and  $\lambda/4$  wave plates is used to compensate for the birefringence, if it is present in the nanowire (the image is taken from Jöns et al. [62]).*



**Figure 6.** QD emission spectra. (a) Emission spectrum by excitation via a green laser. Excitations at two different energy levels, wurtzite InP bandgap at 830 nm and donor/acceptor levels at  $\approx 870$  nm, were used for performing entanglement measurements; (b) the emission spectrum for 830 nm excitation exhibiting the exciton (X), biexciton (XX), and negatively charged exciton ( $X^-$ ) lines. (c) Excitation at to 870 nm leads to an appearance of a positively charged exciton ( $X^+$ ) and suppression of  $X^-$ . The spectra in (b) and (c) were taken at the saturation power of X.

The emission spectrum of the source is provided in **Figure 6**. Upon excitation of the sample using a green laser at  $\lambda = 520$  nm (**Figure 6a**), three sets of peaks can be observed: the wurtzite InP bandgap at  $\lambda = 830$  nm, levels attributed to the donors and acceptors which are formed due to the presence of impurities such as beryllium in the growth chamber, at  $\lambda \approx 870$  nm, and the  $s$ -shell of the QD at  $\lambda \approx 894$  nm. The  $XX - X$  cascade can be generated by exciting the sample either at the InP bandgap or the donor/acceptor levels. The charge environment around the QD is different in the two cases. Whereas excitation at the InP bandgap (**Figure 6b**) leads to appearance of a negatively charged exciton ( $X^-$ ), exciting the QD at the donor/acceptor level will lead to emission of positively charged excitons ( $X^+$ ) and suppression of the  $X^-$  emission line. Moreover, using the donor/acceptor levels to excite the quantum dot, this excitation scheme will fill the charge traps around the QD. As a consequence, the charge mobility will be significantly reduced; a phenomenon which we will show to be extremely effective in suppressing the dephasing caused by the surrounding charge carriers.

Following a similar setup to the one used by Jöns et al. [62] (**Figure 5**), Fognini et al. [45] conducted two-photon quantum state tomography on the  $XX - X$  cascade in time intervals of 100 ps during the decay time of the exciton, which allowed for the construction of the density matrix of the photon pair, and gave the opportunity to observe the evolution of the two photon quantum state. The result of these


**Figure 7.**

Dephasing-free entanglement (a) showing the correlation measurements  $HH + VV$  and  $(RL + LR) - (RR + LL)$ . The former does not show any oscillations as  $|H\rangle$  and  $|V\rangle$  are the eigenstates of the Hamiltonian, whereas the latter reveals the precession of the state between  $|\Psi\rangle$  and  $|\Phi\rangle$ , according to Eq. (2). The shaded gray bars indicate instances with the highest concurrence, (A), and instances with the lowest imaginary part in the density matrix (B-D). (b) The concurrence extracted from the correlation measurements at each instant of time, for time windows of  $\Delta t = 100$  ps, along the decay time of the exciton. (c) Result of the correlations obtained from the theoretical model (Eq. (4)) with the gray shaded bars indicating similar instances as for (a). (d) Comparison of the measured values of the concurrence with that of the theoretical model, revealing the dephasing-free nature of the  $XX - X$  cascade.

measurements with excitation at the donor/acceptor levels can be observed in **Figure 7a, b**. In **Figure 7a**, the results of the correlation measurements in the  $H/V$  basis and  $R/L$  basis are presented. By setting the detector tuned to the  $XX$  emission line as the “start,” and the other detector tuned to  $X$  line as the “stop” in the correlation measurements, variations can be found within the coincidence counts in different bases during the exciton decay. Plotting the correlation counts  $(RL + LR) - (RR + LL)$  vs. decay time reveals the precession of the two-photon quantum state between the two entangled states  $|\Psi\rangle$  and  $|\Phi\rangle$ , according to Eq. (2), with a frequency proportional to  $FSS$ . From a fit to the measured oscillation of the two-photon quantum state, we calculate the  $FSS$  to be  $\delta = 795.52 \pm 0.35$  MHz. From the  $HH + VV$  correlation, a fit to the data yields an  $X$  lifetime of  $\tau_X = 847 \pm 6$  ps. **Figure 7b** shows the results of calculating the concurrence [64],  $\mathcal{C}$ , of the two-photon quantum state, with  $\mathcal{C} = 0$  indicating no entanglement and  $\mathcal{C} = 1$  showing a maximally entangled state, for time windows of 100 ps along the exciton decay time. The gray bars indicate the time instances when the calculated concurrence is the highest, A, and when the imaginary part of the density matrix is zero, B-D. The respective density matrices of each instance is given in the subplots on the top right of **Figure 7**. The concurrence reaches a value of  $\mathcal{C} = 0.77 \pm 0.02$  at its peak, corresponding to a fidelity of  $\mathcal{F} = 0.88$ , with a count-weighted average of  $\bar{\mathcal{C}} = 0.62 \pm 0.03$ .

Despite the fact that the value for concurrence does not reach near unity and that after a peak around  $t = 0$ , it suffers a significant reduction, the observed behavior does not indicate the presence of a dephasing mechanism during the decay time of

the exciton. Fognini et al. [45] further investigated the change of the concurrence value during the exciton's emission time as compared to the measured values with a model that included the parameters of the  $XX - X$  cascade,  $FSS$ ,  $g^{(2)}(0)$  of  $X$  and  $XX$ ,  $\tau_X$ , etc., as well as the features of the detection system, including the detectors' timing resolution and dark counts, but did not include any term for dephasing.

Starting with the state described by Eq. (2), the expected values for 36 possible projection correlations,  $N_{ij}$  ( $i, j \in \{H, V, D, A, R, L\}$ ) with the letters indicating the photon polarization along horizontal, vertical, diagonal, antidiagonal, right, and left, respectively, at time  $t$  and during a time interval  $\Delta t$  can be written as:

$$N_{ij}(t) = N_0 \left( |\langle ij | \Psi(t, \delta) \rangle|^2 n(t, \tau_X) \right) * g(t) \Delta t \quad (4)$$

where  $N_0$  is the total number of photon pairs collected,  $\delta$  is the value of  $FSS$ ,  $\tau_X$  is the lifetime of the exciton state,  $n(t, \tau_X) = 1/\tau_X (e^{-t/\tau_X})$  describes the emission probability of an exciton following an exponential decay,  $*$  is the convolution operator, and  $g(t)$  denotes the detectors' timing resolution function.

To construct the density matrix of the two-photon quantum state, Eq. (4) gives the correlations in all 36 bases with the effect of the detectors' timing resolution function included. However, two additional factors should be included,  $g^{(2)}(0)$  of  $X$  and  $XX$ , and also the detectors' dark counts. The dark counts will result in detection of false correlations that are evenly distributed in time, which has to be added to the raw correlations obtained by Eq. (4). On the other hand, the system studied by Fognini et al. [45] exhibits values of  $g_X^{(2)}(0) = 0.003 \pm 0.003$  for  $X$  and  $g_{XX}^{(2)}(0) = 0.10 \pm 0.01$  for  $XX$  by inclusion of the counts in a range of  $\Delta t = 100$  ps in the proximity of  $t = 0$ . A non-zero value of  $g^{(2)}(0)$  for either  $XX$  or  $X$  results in the addition of uncorrelated photons in the tomography measurement and thus a reduction in the measured entanglement fidelity. Now, by only considering  $g_{XX}^{(2)}(0)$ , since  $g_X^{(2)}(0)$  is negligible in comparison, one finds that uncorrelated photons are being detected in  $g_{XX}^{(2)}(0)$  fraction of the times, which has to be taken into consideration. In other words, the density matrix constructed by considering the correlations in different bases, described in Eq. (4), and addition of the effect of the dark counts describe the behavior of the system only in  $(1 - g_{XX}^{(2)}(0))$  fraction of the times. Therefore, the actual density matrix is expected to be:

$$\rho_{sim}(t) = (1 - g_{XX}^{(2)}(0)) \rho_{raw}(t) + g_{XX}^{(2)}(0) \frac{\mathbb{I}}{4} \quad (5)$$

where  $\rho_{sim}(t)$  is the density matrix of the two-photon quantum state at a particular time  $t$  based on the simulation and after considering all of the factors;  $\rho_{raw}(t)$  is the density matrix constructed from the correlation counts of Eq. (4), together with the effect of the dark counts; and  $\mathbb{I}/4$  is the density matrix of an uncorrelated pair of photons,  $1/4[|HH\rangle\langle HH| + |HV\rangle\langle HV| + |VH\rangle\langle VH| + |VV\rangle\langle VV|]$ .

**Figure 7c** shows the calculated  $HH + VV$  correlations obtained from Eq. (4), as well as  $(RL + LR) - (RR + LL)$  correlations indicating the oscillation between  $|\Psi\rangle$  and  $|\Phi\rangle$ , which shows a similar trend to the experimental results as shown in **Figure 7a**. In the next step, we plot the evolution of the calculated concurrence during the exciton lifetime in **Figure 7d**, based on the density matrix constructed from Eq. (5). The measured values are plotted as light green circles, similar to **Figure 7b**, and the results from the simulation are plotted as a solid red line. Surprisingly, it is with great precision that the two data sets agree. The results from the simulation follow the same trend as the measured values, with three regimes:

(I) top, (II) flat, and (III) roll-off. Initially, as the detectors' response function  $g(t)$  detects more photons, the plot shows an increase in the concurrence reaching a maximum. However, due to the low timing resolution of the detectors after a period of time, the phase averaging of Eq. (2) becomes significant, and the measured concurrence drops. Once the response function has been fully covered, the phase averaging becomes constant, hence reaching the "flat" part. Finally, as the probability of the exciton emission drops exponentially, the effect of dark counts dominates the actual photon counts, and the tomography system will detect uncorrelated false correlations from the dark counts, the part considered as "roll-off" whereby the concurrence drops further. In addition to this close agreement, the count-weighted average concurrence of the simulation yields  $\bar{C}_{\rho_{sim}} = 0.61 \pm 0.01$ , which agrees extremely well with the earlier mentioned value from the measurement,  $\bar{C}_{\rho} = 0.62 \pm 0.03$ , within the error. Thus, the behavior of the two-photon quantum state can be explained by a model which assumes no dephasing, only considering the general features of the source, and the detection systems timing resolution. This indicates that the source at hand is not affected by dephasing during the the exciton decay time once excited at the donor/acceptor level. Hence, this excitation scheme is named "quasi-resonant," as it shows a dephasing-free two-photon quantum state, during the exciton's decay time, without being excited resonantly.

In stark contrast, under non-resonant excitation at the wurtzite InP bandgap, conducting two-photon quantum state tomography reveals the detrimental effect of the surrounding charge noise on the entangled state. By comparing **Figure 8a** and **b**, it becomes clear that shortly after the excitation laser moves to the InP bandgap, the detrimental effects of the excessive charge carriers become evident,  $\approx 0.5$ ns, after the XX emission. Interestingly, these results indicate that during the exciton lifetime, interaction of the exciton state with the charge carriers is the main source of dephasing, not the presence of large nuclear spins, as was generally believed in the community; a finding which is in agreement with a previous work [65], wherein an indium-rich QD was shown not to be affected by the nuclear spins during an exciton lifetime of  $\approx 2.5$ ns.

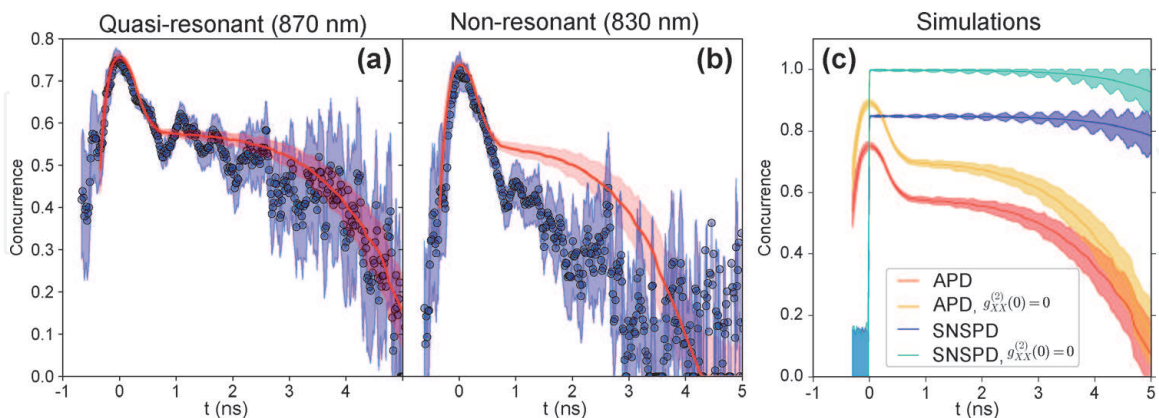


**Figure 8.**

*Effect of the excitation scheme and detection system. (a) Comparison of the theoretical model and results from quasi-resonant excitation indicate suppression of dephasing during the X decay time. (b) Off-resonant excitation at the wurtzite InP bandgap, leads to the mobility of charge carriers and dephasing of the two-photon quantum state shortly after the XX's emission. (c) A combination of two different excitation schemes and detection systems were used to produce the four curves: quasi-resonant excitation and avalanche photodiodes (APDs) (red), resonant TPE and APDs (yellow), quasi-resonant excitation and superconducting nanowire single-photon detectors (SNSPDs) (blue), and resonant TPE and SNSPDs (cyan). Imperfect  $g_{XX}^{(2)}(0)$  values in the case of quasi-resonant excitation (red and blue curves), as well as low timing resolution and relatively high noise level of APDs (red and yellow curves), result in the deterioration of the measured concurrence. Impressively, with the application of resonant TPE, and SNSPDs with a timing resolution of  $\tau_d \sim 30$ ps, and noise level of  $\sim 1$ Hz, the detection of perfect entanglement is expected.*

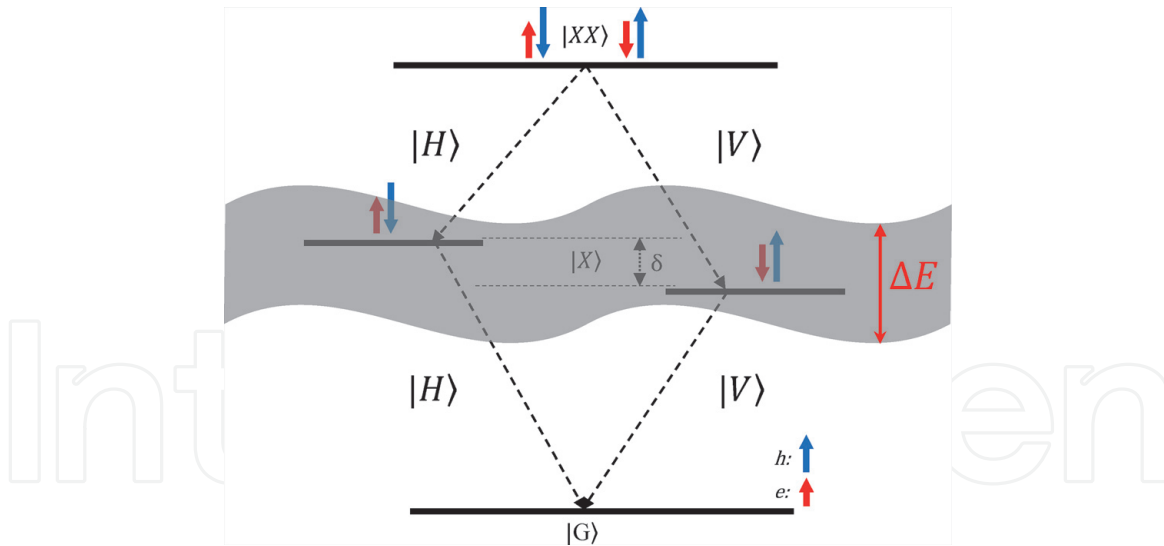
As mentioned earlier, the drop observed in the measured concurrence is the result of the low timing resolution of the detectors. Therefore, it is expected that once the detection system is improved, an enhancement in the measured concurrence will be observed. **Figure 8c** shows the result of a simulation when the features of the detection system and/or the excitation scheme have changed. The red curve shows the actual system at hand, quasi-resonant excitation, with  $g_{XX}^{(2)}(0) = 0.1$ , together with a regular avalanche photodiode (APD) detection system, with a timing resolution of  $\tau_d \sim 300$  ps, with  $\tau_d$  being the FWHM of the response function  $g(t)$ , and with a dark count rate of  $DC \sim 30$  Hz. Upon resonant excitation, the yellow curve, the multiphoton emission of the source is expected to vanish,  $g_{XX}^{(2)}(0) = 0.0$ , and the uncorrelated photons will not enter the analysis, hence, an expected increase in the concurrence value. However, the general shape of the graph does not change. In the case of conducting the experiment with a fast, low-noise detector, such as with superconducting nanowire single-photon detectors (SNSPDs), with a timing resolution of  $\tau_d \sim 30$  ps and a dark count rate of  $DC \sim 1$  Hz, the blue curve, not only will the measured value of the concurrence be enhanced, but the overall shape of the graph will change. The drop in concurrence, observed in the case of APDs, will vanish, and the graph will only consist of the “flat” and “roll-off” parts. However the blue curve still suffers from a non-zero multiphoton emission. But, once the source is excited resonantly, and SNSPDs are used, the cyan curve, remarkably, one expects to measure near-unity concurrence. The count-weighted average concurrence in the latter case is  $\bar{C} = 0.996 \pm 0.008$ .

The way in which the curve of concurrence vs. time is affected by the detectors' response function  $g(t)$  can be analyzed in two equivalent ways. In the first approach, a low timing resolution will result in averaging of the relative phase between the two terms in Eq. (2) and turning the pure two-photon quantum state into a mixed state. In this view, at each particular time  $t$ , the coincidence counts in the range  $[t - \tau_d/2, t + \tau_d/2]$  will be included in the analysis. By dividing this range in shorter time intervals, one can write the resultant measured density matrix,  $\rho_m$ , as:

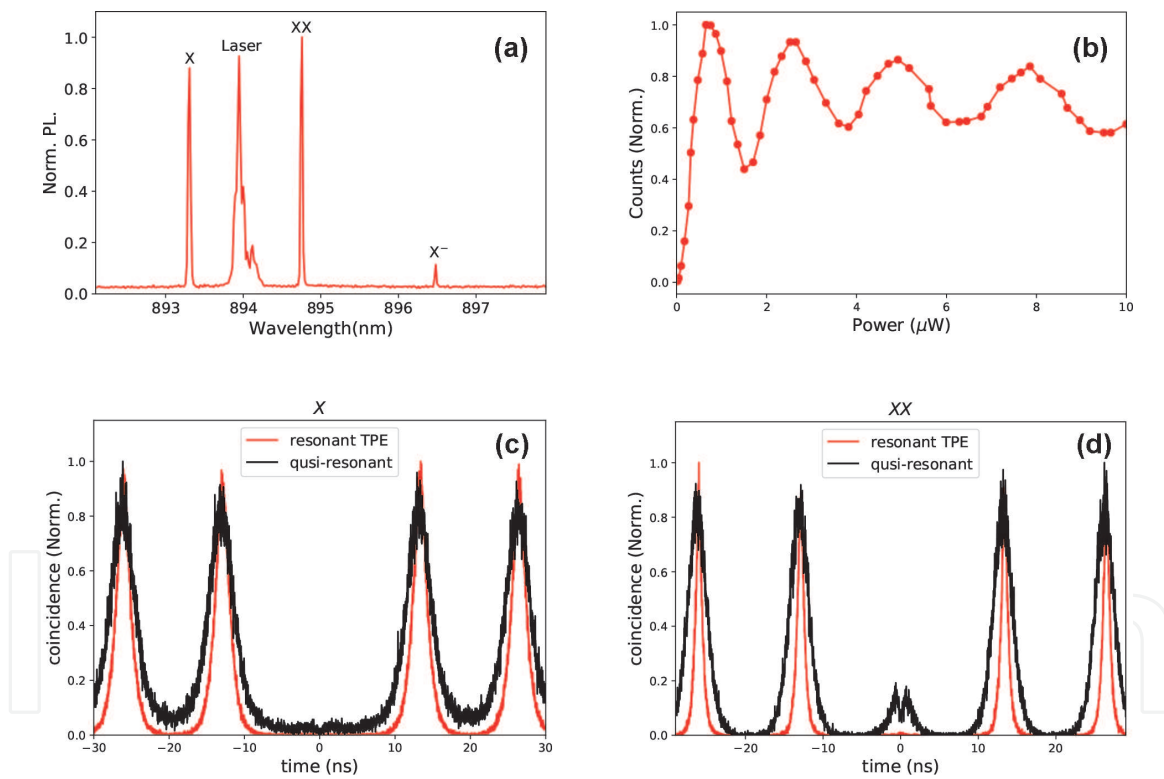
$$\rho_m(t) = \int_{t-\tau_d/2}^{t+\tau_d/2} n(t, \tau_x) \rho(t) dt \quad (6)$$

where  $\rho(t) = |\Psi(t)\rangle\langle\Psi(t)|$  and  $n(t, \tau_x)$  is the probability of the state being in the state  $\rho(t)$ , based on an exponential decay. The rate of change in the density matrix is proportional to the FSS, since FSS results in precession of the state between  $|\Psi\rangle$  and  $|\Phi\rangle$  according to Eq. (2). Therefore, in the case of a large FSS, and a low timing resolution, the measured density matrix will be a result of a mixture of different states in the time interval  $[t - \tau_d/2, t + \tau_d/2]$ . It was found that the time window for tomography analysis can be chosen to be smaller than  $\tau_d$ . In the measurements presented here concerning time windows  $\Delta t < 100$ ps, the concurrence value does not show any change; however, increasing the length of time window above 100 ps reduces the calculated concurrence. This means that the effective time window is slightly less than the FWHM of  $g(t)$ . It is straightforward to see that as the detectors' timing resolution is enhanced,  $\tau_d \rightarrow 0$ , the measured density matrix gets closer and closer to the density matrix of a pure state at each instant of time, hence, an increase in the measured concurrence.

In the alternate approach, the uncertainty in timing of the arrival of the photons can be interpreted as an uncertainty in measuring the energy of  $XX$  and  $X$ , according to  $\Delta\tau_d\Delta E = \hbar/2$ . In this picture, the timing resolution of the detectors competes with the which-path information introduced by the presence of FSS (**Figure 9**). Because of this, a detector with low timing resolution ( $\tau_d \gg \hbar/\delta$ ) will


**Figure 9.**

Detectors' timing resolution and energy uncertainty. The detectors' timing resolution,  $\tau_d$ , directly leads to an uncertainty in the energy of photons,  $\Delta E\tau_d \sim \hbar/2$ . For the case of a fast detector,  $\tau_d \ll \hbar/\delta$ , this uncertainty can smear out the energy difference between the two decay paths and hence retrieve the entanglement, whereas a slow detector,  $\tau_d \gg \hbar/\delta$ , will push the correlations more toward classical correlations.


**Figure 10.**

Resonant two-photon excitation of a nanowire QD. (a) The spectrum of the QD under resonant TPE. The X and XX PL transition rates become more similar as compared to non-resonant excitation, indicating an enhanced pair-production efficiency; and the charged exciton is significantly suppressed, indicating a reduction of excessive charged carriers around the QD. (b) The power-dependent XX count rate exhibits a qualitatively similar Rabi oscillation as the regular direct resonant excitations, qualitatively. (c) and (d) show the comparison between results of  $g^{(2)}(\tau)$  measurements in the case of quasi-resonant and resonant TPE schemes, for X and XX, respectively. Implementation of resonant TPE significantly reduces the emission time jitter of the two states, as well as multiphoton emission of the XX state.

“notice” the energy difference between the two paths, thus degrading the entanglement fidelity. In contrast, a fast detector ( $\tau_d \ll \hbar/\delta$ ) will render the two paths indistinguishable, since the uncertainty in energy will be more than the energy difference of the two paths. In this latter case, the entanglement will be retained and

will reach unity when the detector is fast enough to fully erase the which-path information caused by FSS.

## 2.4 Resonant two-photon excitation

In an attempt to realize on-demand entanglement, we have performed performed resonant two-photon excitation on the same sample used by Fognini et al. [45]. The spectrum of the source under resonant TPE is given in **Figure 10a**. As it is evident from comparing this spectrum with the spectra under non-resonant excitation shown in **Figure 6**, the abundance of charge carriers surrounding the QD is significantly suppressed, leading to a lower intensity of the  $X^-$  line, as compared to  $X$  and  $XX$ . Moreover, the PL transition rates of  $XX$  and  $X$  become closer to each other, a fact that shows an enhancement in pair-production efficiency. By integrating the area under the  $X$  and  $XX$  PL emission lines and calculating their ratio, we have achieved a pair-production efficiency of  $\epsilon_p = 93.6\%$ . Proper population of the  $XX$  state is affected by the center wavelength of the excitation laser, as well as its bandwidth, the length of which can be controlled via a regular 4f pulse shaper. The population of the  $XX$  state in resonant TPE shows a qualitatively similar Rabi oscillation as the regular resonant excitation (**Figure 10b**). The center wavelength and bandwidth of the excitation pulse is chosen so that the  $\pi$  pulse shows the highest possible count rate. Based on taking the setup efficiency and the count rate detected at the  $\pi$  pulse into consideration, the pair-extraction efficiency is reported to be  $\epsilon_e = 12.55\%$ .

Moreover, under resonant TPE, the multiphoton emission is significantly suppressed. **Figure 10c** and **d** show the results of the second-order correlation function performed on the QD once excited at the donor/acceptor levels and under resonant TPE. For resonant TPE,  $g_{XX}^{(2)}(0) = 0.0055 \pm 0.0005$  and  $g_X^{(2)}(0) = 0.0024 \pm 0.0002$ , which demonstrates a two order of magnitude improvement in the case of  $XX$ , as compared to the values reported for quasi-resonant excitation.

## 2.5 State-of-the-art entangled photon sources

The impressive potential for nanowire QDs in detecting entangled photon pairs with near-unity entanglement fidelity is illuminated by the results of the resonant two-photon excitation. Notably, we are now at a point where we can make a comparison between SPDC sources and state-of-the-art QDs in different structures, i.e., self-assembled, micropillar cavities, nanowires, etc. As mentioned earlier, the Poissonian nature of photon-pair emission in SPDC sources limits the performance of such sources to extremely low pair-extraction efficiencies. On the other hand, recent advances in QD growth in various photonic structures have resulted in achieving high entanglement fidelity and high pair-extraction efficiencies, simultaneously. Hüber et al. [67] have reported on measuring an entanglement fidelity of  $F = 0.978(5)$ , from a self-assembled QD by strain-tuning the FSS down to zero. This significant result demonstrates an extensive level of improvement as compared to the results gained from the first generation of self-assembled QDs, where the entanglement fidelity was much lower [38, 68]. The results reported by Fognini et al. [45], in conjunction with the results achieved by resonant TPE, equip us with sufficient information to make such a comparison, the ultimate potential of nanowire QDs in regards to both entanglement fidelity and pair-extraction efficiency, with the values reported for other photonic structures mentioned earlier [26, 32, 33].

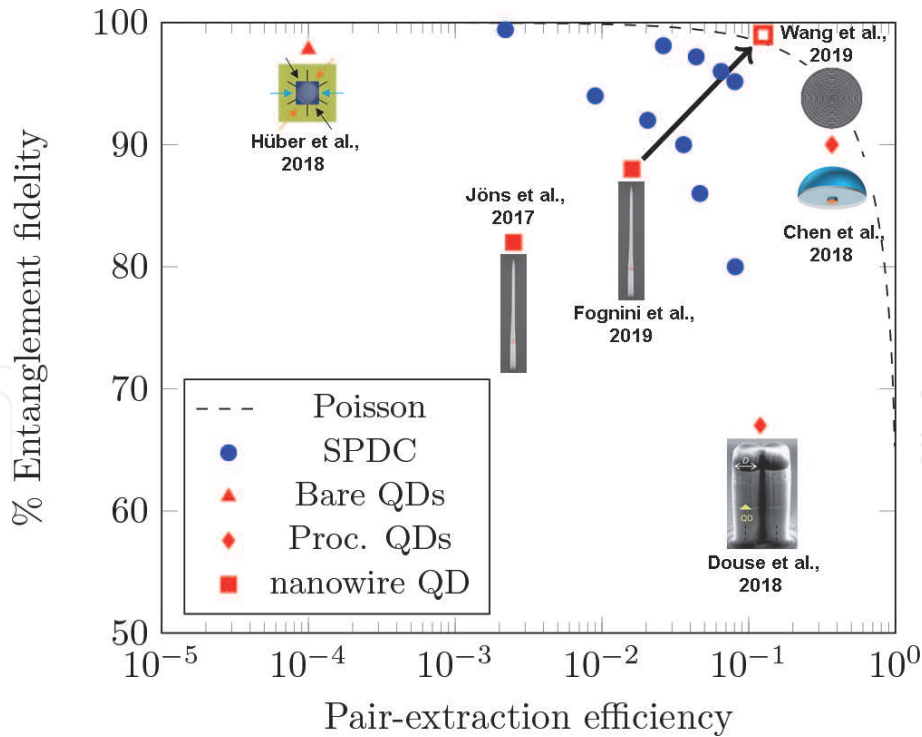


**Figure 11.**

Performance of state-of-the-art entangled photon sources. Comparison between various quantum light sources in terms of entanglement fidelity and pair-extraction efficiency. Blue circles represent SPDC sources, values taken from [69] and [14]. The dashed line shows the ultimate theoretical limit of such sources, with multiphoton emission probability following a Poisson distribution. The red triangle shows results for a bare self-assembled QD, whereas the red diamonds show the results for QDs in different photonic structures. The red solid squares indicate the values reported for nanowire QDs so far. The analysis performed by Fognini et al. [45] and the results obtained by Ahmadi et al. [66] strongly suggest that the sources used for these two studies have the capacity to surpass the performance of SPDC sources once excited via resonant TPE and measured with a fast, low-noise detector. The graph is adapted and modified from [62].

The result of such a comparison is shown in **Figure 11**. The blue circles show different values reported for entanglement fidelity vs. pair-extraction efficiency for SPDC sources. The values are taken from [69] and [14]. The dashed line shows the theoretical limit of such sources, following a Poisson distribution for the probability of multiphoton emission [70]. The two solid red squares indicate the result of two measurements performed on nanowire QDs by Jöns et al. [62] and Fognini et al. [45]. The latter work shows both an improvement in the measured entanglement fidelity and an improvement in pair-extraction efficiency. Based on the results shown by Fognini et al. [45] and the improvements gained by performing resonant TPE, we can predict measuring near-unity entanglement fidelity once two important modifications are implemented: the resonant TPE scheme is employed, and the detection system is improved to a fast and low-noise one. The final result that we predict by implementing these two changes is shown by the hollow red square. This is an extrapolation of results reported thus far on nanowire QDs based on the enhancement achieved in pair-extraction efficiency and entanglement fidelity, as well as the analysis presented in **Figure 8c**. Therefore, it is confidently predicted that nanowire QDs have the potential to surpass and outperform that of SPDC sources, revealing the significant potential of these sources for quantum communication purposes.

### 3. Conclusion and discussion

In this chapter, we have given a historical overview of previous methods for attaining pairs of entangled photons from a QD, as well as included the latest

research and subsequent recent advances toward enhancement of the performance from such sources. Thus far, several photonic structures have been developed in order to improve the low pair-extraction efficiency of self-assembled QDs, among which bottom-up grown nanowire QDs exhibit considerable promise. Based on the detailed studies of these sources under different excitation schemes along with understanding the effects of detection systems and multiphoton emission on the measured value of entanglement fidelity, we predict nanowire QDs can undoubtedly outperform SPDC sources, once excited via resonant TPE and detected by fast, low-noise detectors.

Admittedly, despite the fact that the results that indicate near-unity fidelity are achievable by nanowire QDs, the finite value of  $FSS$  will limit the performance of the source once a particular entangled state is required. In this case, a post selection on the collected photons is inevitable, since the two-photon quantum state precesses between the two entangled states Eq. (2). Strain fields [67], electric fields [40], and magnetic fields [68] are the most popular approaches used for addressing this issue; however, two recent proposals seem to be most compatible with a nanowire QD. The first is the method proposed by Fognini et al. [44], which uses a fast-rotating half-wave plate, realized by an electro-optical modulator, in order to change the energy of the photons after they have been emitted and correct for the energy splitting, thus making this approach a universal  $FSS$  eraser. The second, proposed by Zeeshan et al. [42] on the other hand, corrects the altered symmetry of the exciton's wave function, due to presence of  $FSS$ , via application of a quadrupole electric field, an approach which requires fabrication of electrical gates in the proximity of the nanowire. In addition to  $FSS$  tuning, nanowire QDs have been shown to be integrated into designs realizing performance of on-chip optical operations [71]. Such designs enhance light extraction and also allow for developing scalable quantum photonic circuits, paving the way for performing quantum computational processes on a photonic chip [72], using an on-demand entangled photon source.

Excitingly, this research shows that despite the challenges experienced thus far in generating on-demand and optimally entangled photon pairs, the results gained from resonant excitation of a nanowire QD have in fact revealed the enormous potential these sources have to outperform their predecessors. This research and the realization of optimally entangled photon pairs it offers have given quantum foundations, quantum communication, and quantum information a quantum leap forward.

## Acknowledgements

The authors gratefully acknowledge the Swiss National Science Foundation, Industry Canada, Natural Sciences and Engineering Research Council of Canada (NSERC) and Transformative Quantum Technologies (TQT), for their funding and support.

IntechOpen

### **Author details**

Arash Ahmadi<sup>1\*</sup>, Andreas Fognini<sup>2</sup> and Michael E. Reimer<sup>3</sup>

1 Department of Physics and Astronomy, Institute for Quantum Computing, University of Waterloo, Waterloo, Canada

2 Single Quantum, Delft, Netherlands

3 Department of Electrical and Computing Engineering, Institute for Quantum Computing, Waterloo, Canada

\*Address all correspondence to: arash.ahmadi@uwaterloo.ca

### **IntechOpen**

---

© 2020 The Author(s). Licensee IntechOpen. This chapter is distributed under the terms of the Creative Commons Attribution License (<http://creativecommons.org/licenses/by/3.0>), which permits unrestricted use, distribution, and reproduction in any medium, provided the original work is properly cited. 

## References

- [1] Weston MM, Hall MJW, Palsson MS, Wiseman HM, Pryde GJ. Experimental test of universal complementarity relations. *Physical Review Letters*. 2013; **110**(22):220402
- [2] Shalm LK, Meyer-Scott E, Christensen BG, Bierhorst P, Wayne MA, Stevens MJ, et al. Strong loophole-free test of local realism. *Physical Review Letters*. 2015; **115**(25):250402
- [3] Bouwmeester D, Pan J-W, Mattle K, Eibl M, Weinfurter H, Zeilinger A. Experimental quantum teleportation. *Nature*. 1997; **390**(6660):575
- [4] Pan J-W, Bouwmeester D, Weinfurter H, Zeilinger A. Experimental entanglement swapping: Entangling photons that never interacted. *Physical Review Letters*. 1998; **80**(18):3891
- [5] Ursin R, Tiefenbacher F, Schmitt-Manderbach T, Weier H, Scheidl T, Lindenthal M, et al. Entanglement-based quantum communication over 144 km. *Nature Physics*. 2007; **3**(7):481
- [6] Ekert AK, Rarity JG, Tapster PR, Palma GM. Practical quantum cryptography based on two-photon interferometry. *Physical Review Letters*. 1992; **69**:1293-1295
- [7] Koashi M, Yamamoto T, Imoto N. Probabilistic manipulation of entangled photons. *Physical Review A*. 2001; **63**: 030301
- [8] Qiang X, Zhou X, Wang J, Wilkes CM, Loke T, O’Gara S, et al. Large-scale silicon quantum photonics implementing arbitrary two-qubit processing. *Nature Photonics*. 2018; **12**(9):534
- [9] Burnham DC, Weinberg DL. Observation of simultaneity in parametric production of optical photon pairs. *Physical Review Letters*. 1970; **25**(2):84
- [10] Hong CK, Mandel L. Experimental realization of a localized one-photon state. *Physical Review Letters*. 1986; **56**(1):58
- [11] Shih YH, Sergienko AV, Rubin MH, Kiess TE, Alley CO. Two-photon entanglement in type-II parametric down-conversion. *Physical Review A*. 1994; **50**(1):23
- [12] Verstraete F, Verschelde H. Fidelity of mixed states of two qubits. *Physical Review A*. 2002; **66**(2):22307
- [13] Senellart P, Solomon G, White A. High-performance semiconductor quantum-dot single-photon sources. *Nature Nanotechnology*. 2017; **12**(11): 1026-1039
- [14] Wang X-L, Chen L-K, Wei L, Huang H-L, Liu C, Chao C, et al. Experimental ten-photon entanglement. *Physical Review Letters*. 2016; **117**(21): 210502
- [15] Michler P. *Single Quantum Dots: Fundamentals, Applications and New Concepts*. Vol. 90. Berlin: Springer Science & Business Media; 2003
- [16] Benson O, Santori C, Pelton M, Yamamoto Y. Regulated and entangled photons from a single quantum dot. *Physical Review Letters*. 2000; **84**(11): 2513-2516
- [17] Gywat O, Krenner HJ, Brezovsky J. *Spins in Optically Active Quantum Dots. Concepts and Methods*. Weinheim: WILEY-VCH, KGaA; 2010
- [18] Sipahigil A, Jahnke KD, Rogers LJ, Teraji T, Isoya J, Zibrov AS, et al. Indistinguishable photons from separated silicon-vacancy centers in

- diamond. *Physical Review Letters*. 2014; **113**(11):113602
- [19] Sipahigil A, Goldman ML, Togan E, Chu Y, Markham M, Twitchen DJ, et al. Quantum interference of single photons from remote nitrogen-vacancy centers in diamond. *Physical Review Letters*. 2012; **108**(14):143601
- [20] Koperski M, Nogajewski K, Arora A, Cherkez V, Mallet P, Veuillen J-Y, et al. Single photon emitters in exfoliated WSe<sub>2</sub> structures. *Nature Nanotechnology*. 2015; **10**(6):503
- [21] Tran TT, Bray K, Ford MJ, Toth M, Aharonovich I. Quantum emission from hexagonal boron nitride monolayers. *Nature Nanotechnology*. 2016; **11**(1):37
- [22] Aharonovich I, Englund D, Toth M. Solid-state single-photon emitters. *Nature Photonics*. 2016; **10**(10):631-641
- [23] Leonard D, Krishnamurthy M, Reaves CMV, DenBaars SP, Petroff PM. Direct formation of quantum-sized dots from uniform coherent islands of InGaAs on GaAs surfaces. *Applied Physics Letters*. 1993; **63**(23):3203-3205
- [24] Petroff PM, DenBaars SP. MBE and MOCVD growth and properties of self-assembling quantum dot arrays in III-V semiconductor structures. *Superlattices and Microstructures*. 1994; **15**(1):15
- [25] Watanabe K, Koguchi N, Gotoh Y. Fabrication of GaAs quantum dots by modified droplet epitaxy. *Japanese Journal of Applied Physics*. 2000; **39**(2A):L79
- [26] Chen Y, Zopf M, Keil R, Ding F, Schmidt OG. Highly-efficient extraction of entangled photons from quantum dots using a broadband optical antenna. *Nature Communications*. 2018; **9**(1):1-7
- [27] Gérard JM, Sermage B, Gayral B, Legrand B, Costard E, Thierry-Mieg V. Enhanced spontaneous emission by quantum boxes in a monolithic optical microcavity. *Physical Review Letters*. 1998; **81**(5):1110
- [28] Solomon GS, Pelton M, Yamamoto Y. Single-mode spontaneous emission from a single quantum dot in a three-dimensional microcavity. *Physical Review Letters*. 2001; **86**(17):3903
- [29] Gazzano O, De Vasconcellos SM, Arnold C, Nowak A, Galopin E, Sagnes I, et al. Bright solid-state sources of indistinguishable single photons. *Nature Communications*. 2013; **4**:1425
- [30] Somaschi N, Giesz V, De Santis L, Loredano JC, Almeida MP, Hornecker G, et al. Near-optimal single-photon sources in the solid state. *Nature Photonics*. 2016; **10**(5):340-345
- [31] Rodt S, Heitz R, Schliwa A, Sellin RL, Guffarth F, Bimberg D. Repulsive exciton-exciton interaction in quantum dots. *Physical Review B*. 2003; **68**(3):035331
- [32] Dousse A, Suffczyński J, Beveratos A, Krebs O, Lemaître A, Sagnes I, et al. Ultrabright source of entangled photon pairs. *Nature*. 2010; **466**(7303):217-220
- [33] Wang H, Hu H, Chung T-H, Qin J, Yang X, Li J-P, et al. On-demand semiconductor source of entangled photons which simultaneously has high fidelity, efficiency, and indistinguishability. *Physical Review Letters*. 2019; **122**:113602
- [34] Bayer M, Ortner G, Stern O, Kuther A, Gorbunov AA, Forchel A, et al. Fine structure of neutral and charged excitons in self-assembled In(Ga)As/(Al)GaAs quantum dots. *Physical Review B*. 2002; **65**(19):195315
- [35] Singh R. Tuning fine structure splitting and exciton emission energy in semiconductor quantum dots. *Journal of*

Luminescence. February 2018;**202**:  
118-131

[36] Stevenson RM, Thompson RM, Shields AJ, Farrer I, Kardynal BE, Ritchie DA, et al. Quantum dots as a photon source for passive quantum key encoding. *Physical Review B*. 2002; **66**(8):081302

[37] Santori C, Fattal D, Pelton M, Solomon GS, Yamamoto Y. Polarization-correlated photon pairs from a single quantum dot. *Physical Review B*. 2002; **66**(4):045308

[38] Young RJ, Stevenson RM, Atkinson P, Cooper K, Ritchie DA, Shields AJ. Improved fidelity of triggered entangled photons from single quantum dots. *New Journal of Physics*. 2006; **8**(2):29

[39] Akopian N, Lindner NH, Poem E, Berlatzky Y, Avron J, Gershoni D, et al. Entangled photon pairs from semiconductor quantum dots. *Physical Review Letters*. 2006; **96**(13):130501

[40] Kowalik K, Krebs O, Lemaître A, Laurent S, Senellart P, Voisin P, et al. Influence of an in-plane electric field on exciton fine structure in InAs-GaAs self-assembled quantum dots. *Applied Physics Letters*. 2005; **86**(4):041907

[41] Seidl S, Kroner M, Högele A, Karrai K, Warburton RJ, Badolato A, et al. Effect of uniaxial stress on excitons in a self-assembled quantum dot. *Applied Physics Letters*. 2006; **88**(20):203113

[42] Zeeshan M, Sherlekar N, Ahmadi A, Williams RL, Reimer ME. Proposed scheme to generate bright entangled photon pairs by application of a quadrupole field to a single quantum dot. *Physical Review Letters*. 2019; **122**(22):227401

[43] Trotta R, Zallo E, Ortix C, Atkinson P, Plumhof JD, Van den

Brink J, et al. Universal recovery of the energy-level degeneracy of bright excitons in InGaAs quantum dots without a structure symmetry. *Physical Review Letters*. 2012; **109**(14):147401

[44] Fognini A, Ahmadi A, Daley SJ, Reimer ME, Zwiller V. Universal fine structure eraser for quantum dots. *Optics Express*. 2017; **26**(19):25-28

[45] Fognini A, Ahmadi A, Zeeshan M, Fokkens JT, Gibson SJ, Sherlekar N, et al. Dephasing free photon entanglement with a quantum dot. *ACS Photonics*. 2019; **6**(7):1656-1663

[46] Reimer ME, Bulgarini G, Fognini A, Heeres RW, Witek BJ, Versteegh MAM, et al. Overcoming power broadening of the quantum dot emission in a pure wurtzite nanowire. *Physical Review B*. 2016; **93**(19):1-9

[47] Flagg EB, Polyakov SV, Thomay T, Solomon GS. Dynamics of nonclassical light from a single solid-state quantum emitter. *Physical Review Letters*. 2012; **109**(16):1-5

[48] Michler P. *Quantum Dots for Quantum Information Technologies*. Vol. 237. Berlin: Springer; 2017

[49] Brunner K, Abstreiter G, Böhm G, Tränkle G, Weimann G. Sharp-line photoluminescence and two-photon absorption of zero-dimensional biexcitons in a GaAs/AlGaAs structure. *Physical Review Letters*. 1994; **73**:1138-1141

[50] Flissikowski T, Betke A, Akimov IA, Henneberger F. Two-photon coherent control of a single quantum dot. *Physical Review Letters*. 2004; **92**:227401

[51] Stufler S, Machnikowski P, Ester P, Bichler M, Axt VM, Kuhn T, et al. Two-photon Rabi oscillations in a single In<sub>x</sub>Ga<sub>1-x</sub>As GaAs quantum dot. *Physical*

Review B: Condensed Matter and Materials Physics. 2006;**73**(12):1-7

[52] Jayakumar H, Predojević A, Huber T, Kauten T, Solomon GS, Weihs G. Deterministic photon pairs and coherent optical control of a single quantum dot. *Physical Review Letters*. 2013;**110**:135505

[53] Müller M, Bounouar S, Jöns KD, Glässl M, Michler P. On-demand generation of indistinguishable polarization-entangled photon pairs. *Nature Photonics*. 2014;**8**(3):224-228

[54] Schweickert L, Jöns KD, Zeuner KD, Da Silva SFC, Huang H, Lettner T, et al. On-demand generation of background-free single photons from a solid-state source. *Applied Physics Letters*. 2018; **112**(9):1-4

[55] Claudon J, Bleuse J, Malik NS, Bazin M, Jaffrennou P, Gregersen N, et al. A highly efficient single-photon source based on a quantum dot in a photonic nanowire. *Nature Photonics*. 2010;**4**(3):174

[56] Gregersen N, Nielsen TR, Claudon J, Gérard J-M, Mørk J. Controlling the emission profile of a nanowire with a conical taper. *Optics Letters*. 2008; **33**(15):1693-1695

[57] Reimer ME, Bulgarini G, Akopian N, Hocevar M, Bavinck MB, Verheijen MA, et al. Bright single-photon sources in bottom-up tailored nanowires. *Nature Communications*. 2012;**3**:737

[58] Bulgarini G, Reimer ME, Bavinck MB, Jöns KD, Dalacu D, Poole PJ, et al. Nanowire waveguides launching single photons in a gaussian mode for ideal fiber coupling. *Nano Letters*. 2014;**14**(7):4102-4106

[59] Brown RH, Twiss RQ. A test of a new type of stellar interferometer on sirius. *Nature*. 1956;**178**(4541): 1046-1048

[60] James DFV, Kwiat PG, Munro WJ, White AG. Measurement of qubits. *Physical Review A*. 2001;**64**:052312

[61] Versteegh MAM, Reimer ME, Jöns KD, Dalacu D, Poole PJ, Gulinatti A, et al. Observation of strongly entangled photon pairs from a nanowire quantum dot. *Nature Communications*. 2014;**5**:5298

[62] Jöns KD, Schweickert L, Versteegh MAM, Dalacu D, Poole PJ, Gulinatti A, et al. Bright nanoscale source of deterministic entangled photon pairs violating Bell's inequality. *Scientific Reports*. 2017;**7**(1):1-11

[63] Clauser JF, Horne MA, Shimony A, Holt RA. Proposed experiment to test local hidden-variable theories. *Physical Review Letters*. 1969;**23**(15):880

[64] Bennett CH, DiVincenzo DP, Smolin JA, Wootters WK. Mixed-state entanglement and quantum error correction. *Physical Review A: Atomic, Molecular, and Optical Physics*. 1996; **54**(5):3824

[65] Sénés M, Liu BL, Marie X, Amand T, Gérard JM. Spin Dynamics of Neutral and Charged Excitons in InAs/GaAs Quantum Dots. Dordrecht: Springer Netherlands; 2003. pp. 79-88

[66] Ahmadi A, Mastrovich M, Hosseini S, Jöns KD, Reimer ME. Resonant excitation of a quantum dot in a photonic nanowire. 2020;**5**:3824. Submission in process

[67] Huber D, Reindl M, Filipe S, Schimpf C, Martín-sánchez J, Huang H, et al. Strain-tunable GaAs quantum dot: A nearly dephasing-free source of entangled photon pairs on demand. *Physical Review Letters*. 2018;**121**(3): 33902

[68] Stevenson RM, Young RJ, Atkinson P, Cooper K, Ritchie DA, Shields AJ. A semiconductor source of

triggered entangled photon pairs.  
Nature. 2006;**439**(7073):179-182

[69] Scarani V, de Riedmatten H, Marcikic I, Zbinden H, Gisin N. Four-photon correction in two-photon bell experiments. European Physical Journal D: Atomic, Molecular, Optical and Plasma Physics. 2005;**32**(1):129-138

[70] Daley S. Electro-Optic Rotating Half-Waveplate for a Quantum Dot Fine-Structure Eraser. Ontario: UWSpace, University of Waterloo; 2019

[71] Elshaari AW, Zadeh IE, Fognini A, Reimer ME, Dalacu D, Poole PJ, et al. On-chip single photon filtering and multiplexing in hybrid quantum photonic circuits. Nature Communications. 2017;**8**(1):379

[72] Ma X, Fung C-HF, Lo H-K. Quantum key distribution with entangled photon sources. Physical Review A. 2007;**76**:012307

IntechOpen